PERGAMON

International Journal of Heat and Mass Transfer 44 (2001) 1095–1106

International Journal of HEAT and MASS TRANSFER

www.elsevier.com/locate/ijhmt

# On the use of a low-Reynolds extension to the Chen–Kim ($k$–$\varepsilon$) model to predict thermal exchanges in the case of an impinging plasma jet

Rodolphe Bolot *, Michel Imbert [1], Christian Coddet [2]

*LERMPS – UTBM, 90010 Belfort Cedex, France*

Received 26 September 1998; received in revised form 15 May 2000

**Abstract**

The present paper is devoted to the modeling of an impinging argon/hydrogen plasma jet under atmospheric plasma spraying conditions. A two-layer extension to the Chen–Kim ($k$–$\varepsilon$) turbulence model was implemented in the Phoenics code, allowing the prediction of temperature and velocity fields in the turbulent jet and the description of the viscous sublayer at the surface of the front body. The predictions of thermal exchanges are compared to results obtained with a heuristic formula deduced from experiments and taken from the literature. A comparison is also made with results obtained with some other models and the results indicate that the present proposed model is by far the most accurate. 

## 1. Introduction

Although the standard ($k$–$\varepsilon$) model was originally intended to the study of flows over flat plates, it is often used as a first approximation or for simplicity in many flow situations and particularly for the study of plasma jets [1–11]. Nevertheless, it is known to give poor predictions in a certain number of cases and especially in the case of round jets for which a quite large overestimation of the jet expansion is predicted. For this reason, modifications based on the work of Rodi are sometimes used in order to obtain a better description of round jets [1–3,10]. Nevertheless, the use of those modifications is only possible for free jet studies and not impinging ones, so that the standard ($k$–$\varepsilon$) model is often used without any modification in the case of impinging jets [11–14]. Since it is not valid in laminar boundary layers, this model also uses wall functions in order to describe friction and thermal exchanges with solid bodies. Wall functions are extensively used mainly for the purpose of computational economy. Nevertheless, there are many flow situations in which this approach should not be used, particularly when the boundary layer includes significant variations of thermodynamic properties and transport coefficients, which is especially true in the case of plasma jets. The most used wall function is certainly the logarithmic one [1,11]. Meanwhile, one has to keep in the range of validity of the law and not apply it within the viscous sublayer. Consequently, grid refinement should sometimes be avoided. An alternative approach is the use of low-Reynolds extensions to turbulence models with an adequate grid refinement in the wall region. Numerous extensions to the standard ($k$–$\varepsilon$) model have been proposed in the literature. They differ from the standard model in that local modifications of the constants of the turbulence model are used and that extra source terms are sometimes added to the transport equations of turbulence quantities. Several of those models were described and tested in the case of a simple flow over a flat plate by Patel [15]. Even if those models give good predictions in a range of cases, there are still flow situations in which their use is not recommended. For example, the use of low-Reynolds extensions to

* Corresponding author. Tel.: +33-3-84-58-31-60; fax: +33-3-84-58-32-86.

*E-mail addresses:* rodolphe.bolot@utbm.fr (R. Bolot), michel.imbert@utbm.fr (M. Imbert), christian.coddet@utbm.fr (C. Coddet).

[1] Tel. +33-3-84-58-31-86; fax: +33-3-84-58-32-86.

[2] Tel.: +33-3-84-58-30-23; fax: +33-3-84-58-32-86.

0017-9310/01/$ - see front matter 
PII: S0017-9310(00)00185-X

**Nomenclature**

| | |
|---|---|
| $C_p$ | specific heat |
| $D$ | diffusion coefficient |
| $E_w$ | toughness parameter of the surface |
| $h$ | specific enthalpy |
| $k$ | kinetic energy of turbulence |
| $M$ | molar mass |
| $\dot{m}$ | plasma mass flow rate at the nozzle exit |
| $p$ | pressure |
| $P$ | production rate of $k$ |
| $P_{\text{eff}}$ | net power of the torch |
| $Pr$ | Prandtl number |
| $q$ | energy flux |
| $R$ | nozzle exit radius |
| $Re$ | local Reynolds number |
| $s$ | skin friction factor |
| $Sc$ | Schmidt number |
| $St$ | Stanton number |
| $S_\phi$ | Source term of variable $\phi$ |
| $T$ | temperature |
| $v$ | radial velocity component |
| $v^*$ | resultant frictional velocity |
| $w$ | axial velocity component |
| $x$ | mole fraction |
| $y$ | mass fraction |

*Greek symbols*

| | |
|---|---|
| $\alpha$ | thermal exchange coefficient |
| $\varepsilon$ | rate of dissipation of $k$ |
| $\kappa$ | Von-Karman constant |
| $\lambda$ | thermal conductivity |
| $\mu$ | dynamic viscosity |
| $\nu$ | kinematic viscosity |
| $\rho$ | density |
| $\sigma_\phi$ | turbulent Prandtl number of variable $\phi$ |
| $\Gamma_\phi$ | exchange coefficient of $\phi$ |
| $\tau_w$ | shear stress at the wall |

turbulence models in the case of separating and reattaching flows and in the case of impinging flows can lead to a significant overestimation of thermal exchanges. To compensate this deficiency, Yap [16] proposed to add a source term to the $\varepsilon$ equation in order to drive the length scale toward its local equilibrium value near a wall. Modifications proposed by Yap are generally used in the case of impinging flows [13]. A second possibility is the use of a two-layer model [17]. By doing so, a two-equation model is used except near a wall where a one-equation model with a prescription of the length scale is preferred. Two layers models are particularly recommended for impinging flow situations and represent a good alternative to the use of a low-Reynolds extension combined with the Yap correction source term. In the present study, a two-layer extension to the $(k$–$\varepsilon)$ turbulence model by Chen and Kim was implemented in the Phoenics code. The choice of the Chen–Kim model [18,19] was decided regarding to its particular performances for round jets modeling, whereas the two-layer extension was implemented in order to obtain a good description of the viscous sublayer at the surface of the front plate.

## 2. Mathematical model

In a direct current (D.C.) arc plasma torch, the plasma gas mixture flowing through the torch is accelerated, heated and partially ionized under the effect of an electric arc created between a cathode and an anode both cooled by a water circuit. In the present model, we studied the plasma jet from the torch exit to its impingement on a front plate. Velocity and enthalpy profiles at the torch exit were firstly determined in order to satisfy the gas flow rate and the net power input (deduced from the knowledge of the electric power and that of the cooling). The plasma was assumed to be in local thermodynamic equilibrium (LTE) and was considered as optically thin. The case of an argon/hydrogen plasma jet discharging into air was considered and properties of the argon/hydrogen plasma and the surrounding air were calculated separately assuming chemical equilibrium. Chemical reactions between those two mixtures were then neglected. Since the nature of the surrounding gas is known to have an important influence on the cooling of the plasma jet in the environment, the mixing of the plasma jet in the surrounding air was described using a mass fraction conservation equation [1,3–5,8–11] (similar to a species conservation equation). Nevertheless, in the present model, demixing effects were neglected on the contrary to the one proposed by Fincke [6], but this is not the originality of the present paper which deals with turbulence modeling as much as with plasma jets.

### 2.1. Thermodynamic properties and transport coefficients

A Gibbs free energy minimization method based on the RAND algorithm [20] and modified in order to take the presence of free electrons into account [21] was used in order to calculate the chemical equilibrium composition of air and that of the argon/hydrogen spray gas mixture. Required thermodynamic properties of individual substances were taken from Gurvich's tables [22], the advantage of which being the range of temperature

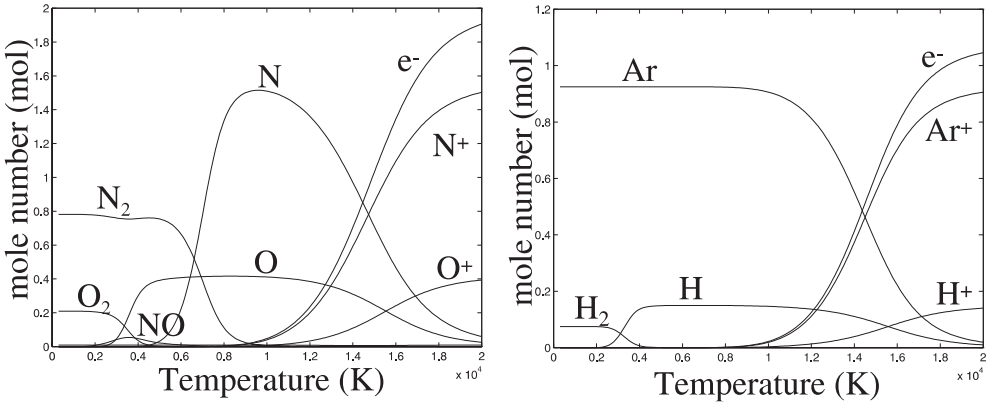


Fig. 1. Chemical equilibrium composition of air and argon/hydrogen (92.5/7.5) versus temperature at 0.1 MPa (for 1 initial mole at 300 K).

considered (0–20 000 K). Thermodynamic properties of the two mixtures were then deduced from the chemical equilibrium composition by summation over the species for enthalpy and numerical derivation of enthalpy for the specific heat, whereas transport coefficients were calculated, according to kinetic theory of gases, assuming different interaction potentials between each pair of species. For this part, exponential repulsive potentials were used for neutral–neutral interactions, the screened Coulomb potential was used for charged–charged interactions, the polarization potential was used for neutral–ion interactions and collision integral tabulations were used for neutral–electron interactions whereas resonant charged transfer influence was also taken into account for interactions between atoms and their associated positive ions (see [21] for a complete description). Data taken from references indicated by Murphy [23,24] were mainly used concerning potentials for transport coefficients of air, whereas potentials proposed by Pateyron et al. [25] were used concerning the argon/hydrogen mixture. As a consequence, results obtained for transport coefficients are very similar to those proposed in those references. Fig. 1 presents the chemical equilibrium composition of air and of the argon/hydrogen (92.5/7.5) mixture versus temperature at 0.1 MPa. For low temperatures, components are present only in their ground state in the mixtures, whereas they are progressively dissociated and ionized when the temperature increases.

Fig. 2 presents enthalpy, specific heat, dynamic viscosity and thermal conductivity of each one of the two mixtures. In order to keep the problem computationally reasonable, approximate mixing rules were used to estimate properties of the mixture of plasma gas and air. The mixing rules used for dynamic viscosity and thermal conductivity were $\mu = x_1\mu_1 + x_2\mu_2$ and $\lambda = x_1\lambda_1 + x_2\lambda_2$ in which indices 1 and 2 stand for plasma spray gas and air, respectively, except in the boundary layer close to the solid body (front plate) for which the Wilke mixing rule [25] (which is more realistic for temperatures at which species are fully recombined) was preferred for both dynamic viscosity and thermal conductivity.

The use of those mixing rules can be expected to have only a small influence for different reasons: firstly, the viscosity of the argon/hydrogen mixture and that of air (Fig. 2) are not so different from one another whatever the temperature range, and secondly and mainly, turbulence effects are dominant except in the potential core of the jet and in the laminar region close to the solid body.

### 2.2. Governing equations

A cylindrical geometry with coordinates $(r,z)$ was used and axial symmetry was imposed so that the $\theta$ gradient was omitted from equations (2D calculation). Finally, the considered equations were the following:

*Continuity*

$$\frac{1}{r}\frac{\partial \rho r v}{\partial r} + \frac{\partial \rho w}{\partial z} = 0. \tag{1a}$$

*Axial momentum*

$$\frac{1}{r}\frac{\partial \rho r v w}{\partial r} + \frac{\partial \rho w^2}{\partial z} - \frac{1}{r}\frac{\partial}{\partial r}\left(r\mu_e \frac{\partial w}{\partial r}\right) - \frac{\partial}{\partial z}\left(\mu_e \frac{\partial w}{\partial z}\right) = -\frac{\partial p}{\partial z} + \frac{\partial}{\partial z}\left(\mu_e \frac{\partial w}{\partial z}\right) + \frac{1}{r}\frac{\partial}{\partial r}\left(r\mu_e \frac{\partial v}{\partial z}\right). \tag{1b}$$

*Radial momentum*

$$\frac{1}{r}\frac{\partial \rho r v^2}{\partial r} + \frac{\partial \rho w v}{\partial z} - \frac{1}{r}\frac{\partial}{\partial r}\left(r\mu_e \frac{\partial v}{\partial r}\right) - \frac{\partial}{\partial z}\left(\mu_e \frac{\partial v}{\partial z}\right) = -\frac{\partial p}{\partial r} + \frac{\partial}{\partial z}\left(\mu_e \frac{\partial w}{\partial r}\right) + \frac{1}{r}\frac{\partial}{\partial r}\left(r\mu_e \frac{\partial v}{\partial r}\right) - 2\mu_e \frac{v}{r^2}. \tag{1c}$$

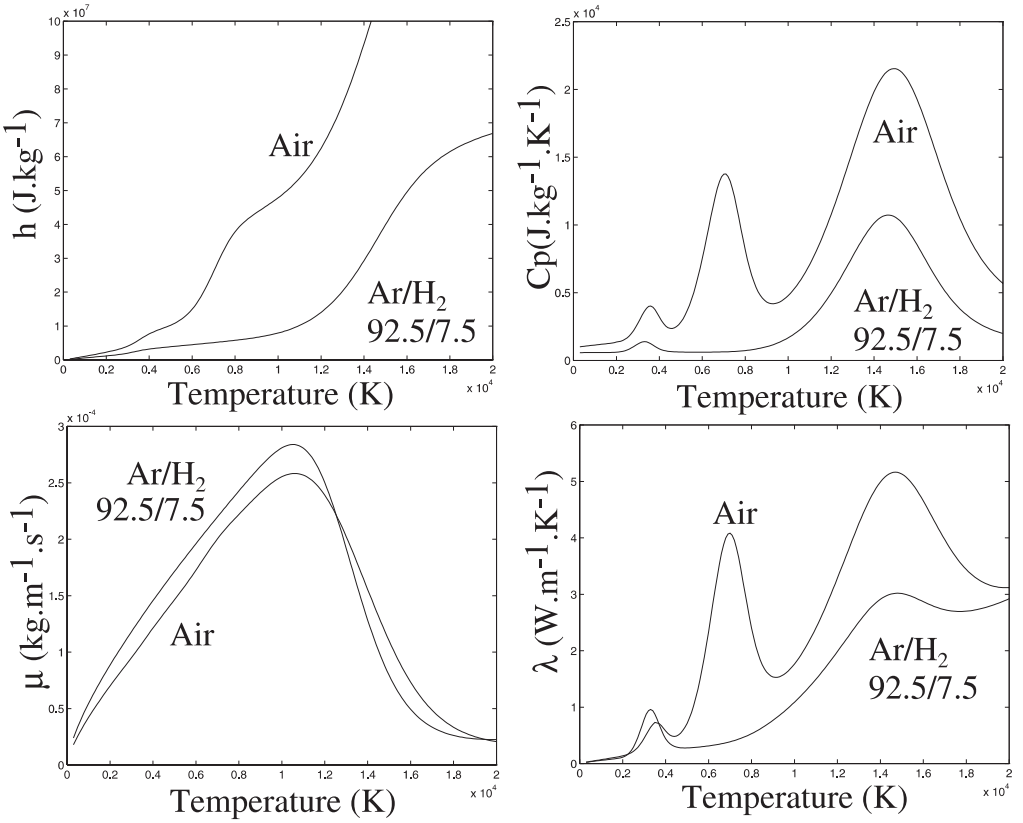


Fig. 2. Thermodynamic properties and transport coefficients of air and argon/hydrogen (92.5/7.5) versus temperature at 0.1 MPa.

*Energy*

$$\frac{1}{r}\frac{\partial \rho r v h}{\partial r}+\frac{\partial \rho w h}{\partial z}-\frac{1}{r}\frac{\partial}{\partial r}\left(r\Gamma_h\frac{\partial h}{\partial r}\right)-\frac{\partial}{\partial z}\left(\Gamma_h\frac{\partial h}{\partial z}\right)=v\frac{\partial p}{\partial r}+w\frac{\partial p}{\partial z}+\mu_e\phi_v. \tag{1d}$$

*Mass fraction of argon/hydrogen*

$$\frac{1}{r}\frac{\partial \rho r v y_1}{\partial r}+\frac{\partial \rho w y_1}{\partial z}-\frac{1}{r}\frac{\partial}{\partial r}\left(r\Gamma_y\frac{\partial y_1}{\partial r}\right)-\frac{\partial}{\partial z}\left(\Gamma_y\frac{\partial y_1}{\partial z}\right)=0. \tag{1e}$$

*Turbulence kinetic energy*

$$\frac{1}{r}\frac{\partial \rho r v k}{\partial r}+\frac{\partial \rho w k}{\partial z}-\frac{1}{r}\frac{\partial}{\partial r}\left(r\Gamma_k\frac{\partial k}{\partial r}\right)-\frac{\partial}{\partial z}\left(\Gamma_k\frac{\partial k}{\partial z}\right)=\rho(P-\varepsilon). \tag{1f}$$

*Turbulence kinetic energy dissipation rate*

$$\frac{1}{r}\frac{\partial \rho r v \varepsilon}{\partial r}+\frac{\partial \rho w \varepsilon}{\partial z}-\frac{1}{r}\frac{\partial}{\partial r}\left(r\Gamma_\varepsilon\frac{\partial \varepsilon}{\partial r}\right)-\frac{\partial}{\partial z}\left(\Gamma_\varepsilon\frac{\partial \varepsilon}{\partial z}\right)=\frac{\rho\varepsilon}{k}\left(C_1P-C_2\varepsilon+C_3\frac{P^2}{\varepsilon}\right) \tag{1g}$$

in which

$$\mu_e=\mu+\mu_t,\quad \Gamma_h=\frac{k}{Cp}+\frac{\mu_t}{Pr_t},\quad \Gamma_y=\rho D+\frac{\mu_t}{Sc_t}$$

and

$$\Gamma_k=\mu+\frac{\mu_t}{\sigma_k},\quad \Gamma_\varepsilon=\mu+\frac{\mu_t}{\sigma_\varepsilon},\quad \mu_t=\rho C_\mu\frac{k^2}{\varepsilon}.$$

$P$ the rate of production of $k$ and $\phi_v$ the dissipation function can be expressed in terms of velocity gradients by

$$\rho P=\mu_t\phi_v=\mu_t\left[\left(\frac{\partial w}{\partial r}+\frac{\partial v}{\partial z}\right)^2+2\left(\frac{\partial w}{\partial z}\right)^2+2\left(\frac{\partial v}{\partial r}\right)^2+2\left(\frac{v}{r}\right)^2\right].$$

In view of the difficulty to define the diffusion coefficient of one mixture into an other (each one containing in fact different species), a unitary Lewis number was assumed as first approximation in order to estimate the diffusion coefficient of the spray gas in the ambient air ($Le=Sc/Pr=k/\rho C_pD=1$).

Table 1
Turbulent parameters used in the Chen–Kim model

| $C_\mu$ | $C_1$ | $C_2$ | $C_3$ | $\sigma_k$ | $\sigma_\varepsilon$ |
|---|---|---|---|---|---|
| 0.09 | 1.15 | 1.90 | 0.25 | 0.75 | 1.15 |

This assumption also leads to some simplifications in the energy conservation equation since, as it can be seen in Eq. (1d), the source term

$$\mathrm{div}\left[\left(\frac{\mu}{Sc}\left(1-\frac{Sc}{Pr}\right)+\frac{\mu_t}{Sc_t}\left(1-\frac{Sc_t}{Pr_t}\right)\right)(h_1-h_2)\vec{\nabla}y_1\right]$$

resulting from inter-diffusion of the two gases was omitted (the same value of the turbulent Prandtl and Schmidt numbers being also used). This final form of the energy equation results from the combination of the term of heat diffusion due to the temperature gradient and the term of inter-diffusion of the two gases [11].

The $(k$–$\varepsilon)$ turbulence model of Chen and Kim differs from the standard one in that the additional source term $C_3\rho(P^2/k)$ is included to the $\varepsilon$ in Eq. (1g). According to the authors [18], this extra source term represents energy transfer from large-scale to small-scale turbulence controlled by the production range time scale and the dissipation range time scale. In addition, several of the standard model constants were adjusted so that the model maintains good agreement with the experimental data for classical cases. Table 1 presents the turbulence parameters used in the turbulence model by Chen and Kim.

Moreover, in the present study, a value of 0.7 was used for the turbulent Prandtl and Schmidt numbers. This is in agreement with suggestions by Lee and Pfender [10] for plasma jets and by Schiestel [26] for circular jets in general. The use of a smaller value than that used in [4,5,8,11] is justified in that sense that a value of 0.9 was used in those works mainly to compensate the influence of the use of the standard $(k$–$\varepsilon)$ model which tended to overestimate the jet expansion and to predict a too fast temperature decrease. This is not necessary anymore with the Chen–Kim model.

### 2.3. Boundary conditions

Fig. 3 presents a view of the computational domain. The previous set of equations (1a)–(1g) can be written in the form $\vec{\nabla}\cdot(\rho\vec{V}\phi-\Gamma_\phi\vec{\nabla}\phi)=S_\phi$, where the first term $\rho\vec{V}\phi$ is the convective term, the second one $-\Gamma_\phi\vec{\nabla}\phi$ is the diffusive term and $S_\phi$ is the source term of the solved variables $\phi$. In the Phoenics code (which was used for the computations), the convective and diffusive terms are omitted on cell faces pertaining to each boundary, assuming negligible normal gradients and normal velocity component. A different boundary condition must be specified by the way of a source term added to the concerned finite volume equation. As a first consequence, the case of a symmetry axis for example does not require any additional source term.

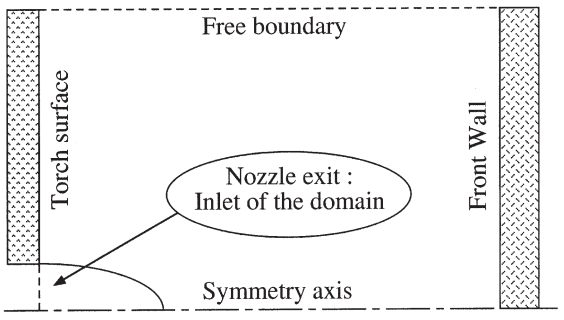


Fig. 3. View of the computational domain.

#### 2.3.1. At the free boundary

For the free boundary (Fig. 3), the mass flux passing through the domain is calculated from the pressure prevailing in the cell and the one specified at the boundary (fixed pressure boundary condition). Properties of the incoming fluid were prescribed as that of pure air at 300 K (with a zero concentration of the plasma gas). Since the "upwind assumption" is used at the boundary, specified properties for the incoming fluid have no influence for cells at which outflow occurs.

#### 2.3.2. At the nozzle exit

As already used in [8] or [11], we assumed velocity and enthalpy profiles of the form

$$\phi(r)-\phi_w=(\phi_{cl}-\phi_w)\left[1-\left(\frac{r}{R}\right)^n\right]$$

at the torch exit (inlet of the domain), where $w_{cl}$ and $h_{cl}$ (the velocity and enthalpy on the centerline) were determined from global mass and total enthalpy conservation and $h_w$ (the enthalpy at the wall) was fixed to a value corresponding to a temperature of 1100 K (which is close to the assumption used for example by Murphy et al. [1]). The mass and total enthalpy conservation represents a system of two equations with two unknowns ($w_{cl}$ and $h_{cl}$) if a zero pressure is assumed at the nozzle exit and if the shape of the profile is decided. An iterative method was used in order to deduce the centerline values of the velocity and enthalpy from this system formed by

$$\dot{m}=\int_0^R\rho(r)w(r)2\pi r\,\mathrm{d}r \text{ and}$$

$$P_{\mathrm{eff}}=\int_0^R\rho(r)w(r)[h(r)+w(r)^2/2-h_{300\ \mathrm{K}}]2\pi r\,\mathrm{d}r.$$

A value of $n=3$ was used in the expression of $\phi(r)$ for velocity and enthalpy. It ensured that subsonic

conditions were specified over the nozzle exit section. This value is of the same order as that used by Diliwari and his co-workers for example [3–5]. One can also notice that for a given enthalpy profile, the corresponding temperature profile is always much flatter (the reason being the increase of the specific heat of thermal plasma at high temperatures). This tendency is in accordance with suggestions by Vardelle et al. [27–30] who used $n = 2$ for velocity and $n = 4.5$ for temperature or by Nylén [31]. Another indication concerning the validity of the present nozzle exit conditions was obtained considering the recently published velocity measurements by Planche et al. [32–34] in the near nozzle exit region. For experimental conditions considered in [34], the nozzle exit velocity computed with the present model compares well with measurements. Moreover, the influence of nozzle exit profiles is reduced when the distance from the nozzle exit increases so that one can expect that it does not significantly change the prediction of thermal exchanges with the front plate. One should also notice that although an accurate modeling of the flow inside the torch would perhaps give a better idea of the nozzle exit conditions, the present model is the only one which ensures that the true efficient power is given to the external jet (since the efficiency of the torch is deduced from experiments, it is not sensitive to the validity of the model).

One has also to specify turbulence quantities over the nozzle exit. This was done according to Fincke [6] who assumed proportionality between the radial gradient of axial velocity and the turbulence kinetic energy. Finally, the turbulence kinetic energy profile was fixed

$$k(r) = \mathrm{it}\, w_{\mathrm{cl}}^2 \left(\frac{\partial w}{\partial r}\right) \Big/ \left(\frac{\partial w}{\partial r}\right)_R$$

with $\mathrm{it} = 0.003$, whereas its dissipation rate was given by

$$\varepsilon(r) = C_\mu^{3/4} k(r)^{3/2}/l \quad \text{with } l = \min(\kappa(R-r), 0.07R).$$

In this expression $\kappa$ is the Von-Karman constant taken as 0.41 in the present study.

The above set of equations leads to sufficiently small values of turbulence quantities so that the laminar viscosity significantly exceeds the resulting turbulent one especially in the centerline region of the jet.

### 2.3.3. For the torch surface

The source term to be added to represent a wall requires the knowledge of the skin friction factor. For the torch surface (perpendicular to the main flow at the nozzle exit), the standard log law of the wall was used. By doing so, the skin friction factor at the solid surface $s = \tau_{\mathrm{w}}/(\rho v^2) = (v^*/v)^2$ is determined using an iterative procedure from $s^{1/2} = \kappa/\ln(E_w\, z^+)$, where $z^+ = Re_w s^{1/2}$ and $Re_w = \rho v d_{1/2}/\mu$. In those expressions, $E_w$ is the characteristic roughness parameter of the surface (8.6 for example in the case of a smooth surface), $d_{1/2}$ is the distance from the center of the cell to the wall, $\tau_{\mathrm{w}}$ is the shear stress at the wall and $v^*$ is the resultant frictional velocity. The range of validity of this law concerns the logarithmic region only and does not include the viscous sublayer. In order to compensate somewhat this deficiency, the final skin friction factor is determined from the maximum between the one deduced from the above formula and the one representing a laminar flow $s = 1/Re_w$. Turbulence quantities at the wall are then specified following:

$$k_{\mathrm{w}} = \frac{\tau_{\mathrm{w}}}{\rho\sqrt{C_\mu}} = \frac{|v^*|^2}{\sqrt{C_\mu}}$$

and

$$\varepsilon_{\mathrm{w}} = C_\mu^{3/4} \frac{k_{\mathrm{w}}^{3/2}}{\kappa d_{1/2}} = \frac{|v^*|^3}{\kappa d_{1/2}},$$

whereas the Stanton number for the energy equation is calculated from

$$St = \frac{s}{Pr_t\left(1 + 9.0((Pr_l/Pr_t) - 1)(Pr_t/Pr_l)^{1/4} s^{1/2}\right)}.$$

### 2.3.4. At the front plate

The use of the logarithmic law in order to describe friction on the torch surface is accurate since it has little effect on the jet modeling. Unfortunately, this is not the case of the impinging region for which this approach was found to give poorly realistic results [11]. In order to compensate this deficiency and to obtain accurate predictions of thermal exchanges, a two-layer modification was implemented in the code in order to describe friction on the front plate. By doing so, the high-Reynolds form of the turbulence model is used, except close to the solid body where a one-equation turbulence model with a prescription of the length scale is applied. This procedure is useful since the length scale distribution is quite well defined near a wall. Two-layer extensions have been extensively developed for the standard $(k$–$\varepsilon)$ model and not for the Chen–Kim one. Meanwhile, since the two models (the standard one and the Chen–Kim one) use the same value of $C_\mu$, the two-layer extension proposed by Rodi [17] for the standard model was also applied to the Chen–Kim one. In this model, the rate of dissipation of the turbulence kinetic energy is fixed to

$$\varepsilon = C_\mu^{3/4} \frac{k^{3/2}}{l_m} F_2$$

within the viscous sublayer. In this equation,

$$F_2 = 1 + \frac{5.3}{R_k} \quad \text{and} \quad R_k = \frac{\rho\sqrt{k}d_w}{\mu}$$

in which $d_w$ is the distance from the point in question to the wall and $l_m$ is deduced from the near wall formula ($l_m = \kappa d_w$). The effective turbulent dynamic viscosity is then deduced from

$$\mu_t = C_\mu^{1/4}\rho k^{1/2} l_m F_\mu = C_\mu \rho \frac{k^2}{\varepsilon} F_\mu F_2 \quad \text{with}$$
$$F_\mu = 1 - \exp(-0.0198 R_k).$$

Since the turbulence model is now accurate in the viscous sublayer, an important grid refinement can be used at the surface, so that the skin friction factor and the Stanton number can be calculated from their laminar expressions $s = 1/Re_w$ and $St = s/Pr_l$, the associated boundary conditions for the transport equation of the kinetic energy of turbulence being $k = 0$ at the wall. The transition between the two regions ($\varepsilon$ solved or $\varepsilon$ fixed) is defined for a local Reynolds number $Re_w$ of 350. The thermal flux is then calculated from $q = \lambda(T - T_w)/d_{1/2} = St\,\rho v(h - h_w)$, where $h_w$ is the corresponding wall enthalpy. In the present study, we assumed a temperature of 300 K at the surface of the solid structure.

The use of this two-layer extension to the Chen–Kim model was preferred to the Lam–Bremhorst low-Reynolds extension [35] to the Chen–Kim model essentially for one reason: even if the Chen–Kim model is known to give better results than the standard one in the case of flows, where turbulence is removed from equilibrium, its Lam–Bremhorst low-Reynolds extension was found to have still the same major default as all low-Reynolds extension models *when used without the Yap correction source term*. That is to say that they predict progressively too high values of the length scale inside the boundary layer in the case of impinging flows, resulting in a quite large overestimation of thermal fluxes. This effect was found to be weak for short stand-off distances (of the order of 50 mm), but it increases for higher ones to give about twice the thermal exchange values obtained with the two-layer model for a stand-off distance of the order of 100 mm. On the contrary, it was verified that the use of the Lam–Bremhorst low-Reynolds extensions to the standard ($k$–$\varepsilon$) model coupled with the Yap correction source term leaded to similar results to those obtained with the two-layer extension to this model [21]. This confirms the validity of the use of a two-layer extension since the use of the Yap correction source term is considered to be the best solution in order to represent impinging flows correctly. Moreover, it indicates that although the high-Reynolds form of the turbulence model is used in the potential core of the jet (laminar region), this has no influence on the predictions.

### 2.4. Source terms for turbulence quantities

As said previously, the Phoenics code was used for the resolution of the set of equations (1a)–(1g). It uses a finite volume formulation in which scalar quantities are calculated at cell centers and velocity components are calculated at cell faces. The discretization equations [36] result in an algebraic system of the form $a_p\phi_p = \sum_{nb} a_{nb}\phi_{nb} + b$, where nb stands for neighbors to cell $P$ and where $b$ includes the contribution of source terms.

Source terms are all implemented by the same way. That is to say that they are written in the form $S_\phi = S_{\phi c} - S_{\phi p}\phi = C(V - \phi)$, so that the positive part is let in the right-hand side of the algebraic equation and the other part is moved in the left-hand side (where it increases the value of $a_p$). Although the linearization of source terms should not affect the final solution, it has an important influence on the time required to achieve convergence and can even sometimes prevent from any convergence. A particular attention is so required concerning the linearization of source terms for turbulence quantities. In order to avoid conflicts with the different built-in options of Phoenics, source terms were fully rewritten following:

$$\frac{S_k}{\rho} = P - \varepsilon = C_\mu \frac{k}{\nu_t} F_\mu F_2 \left( \frac{1}{C_\mu}\frac{P}{k}\nu_t \frac{1}{F_\mu F_2} - k \right)$$

and

$$\frac{S_{1\varepsilon}}{\rho} = \frac{\varepsilon}{k}(C_1 P - C_2\varepsilon) = C_2 C_\mu \frac{k}{\nu_t}\left(\frac{C_1}{C_2}P - \varepsilon\right),$$

where $\nu_t = \mu_t/\rho$ is the turbulent kinematic viscosity. Since $\varepsilon$ is solved only in regions where $F_\mu = F_2 = 1$, this expression of $S_{1\varepsilon}$ is correct. One can then easily identify $C$ and $V$ in the previous expression of $S_\phi$. The additional term $S_{2\varepsilon}/\rho = C_3 P^2/k$ was included without any linearization.

10 000 cells were typically used in order to build the mesh and the required computational time was significantly increased when compared to the one spent for a free jet simulation, the main reason being that the time step used in the relaxation procedure had to be reduced in view of the mesh refinement in the wall region (in which a minimum of 20% of the total number of grid points are concentrated). Moreover, the case of a free jet can be accurately described using a parabolic assumption [8] (so that a more economical z-marching procedure could be used). Finally, the required computational time to obtain a sufficiently high rate of convergence exceeds 3 h using a RISC 6000/43P with 128 Mo RAM for such a case, so that a 3D calculation would not be reasonable.

## 3. Numerical results

The numerical results presented here concern an experimental case for which a commercial Sulzer–Metco F4 plasma torch was used. In order to be able to compare the turbulence models, the same parameters as those used in [11] were chosen. The nozzle diameter was 6 mm, the plasma gas was a mixture of argon (37 slpm) and hydrogen (3 slpm), whereas the net power (deduced from the electric power and the torch efficiency) was 16500 W. Computations were realized for three different positions of the plate (80, 100 and 125 mm from the nozzle exit) and in each case, a temperature of 300 K was assumed at the surface of the plate.

Figs. 4–7 show the results obtained from computations realized with the two-layer extension to the Chen–Kim ($k$–$\varepsilon$) model for the stand-off distance of 80 mm.

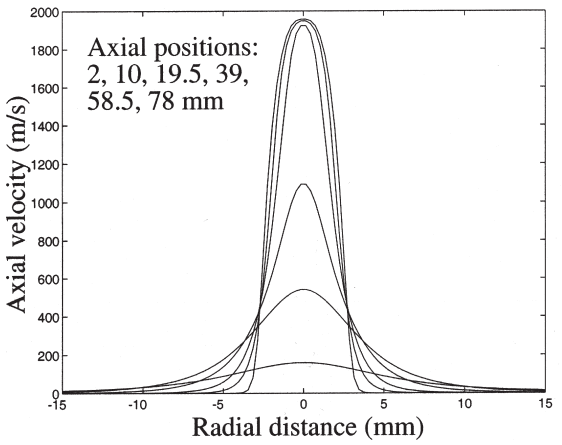


Fig. 4. Radial profiles of axial velocity for a stand-off distance of 80 mm computed with the Chen–Kim model.

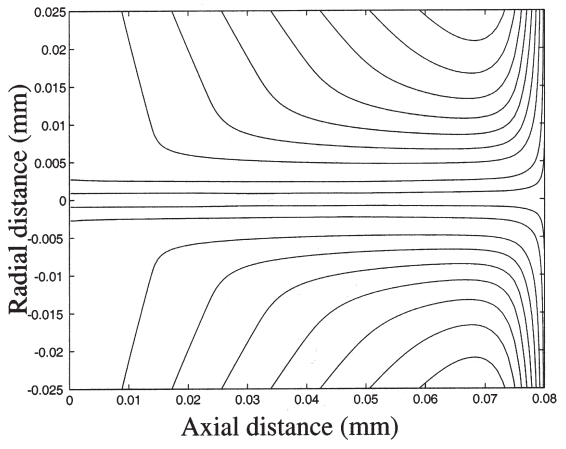


Fig. 5. Streamlines computed with the two-layer extension to the Chen–Kim ($k$–$\varepsilon$) model for a stand-off distance of 80 mm.

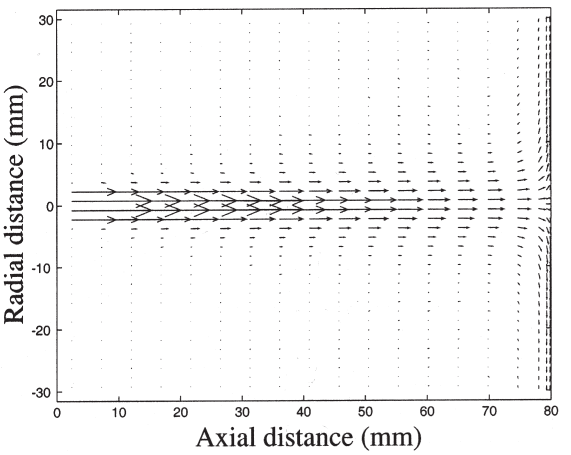


Fig. 6. Velocity vectors computed with the two-layer extension to the Chen–Kim ($k$–$\varepsilon$) model for a stand-off distance of 80 mm.

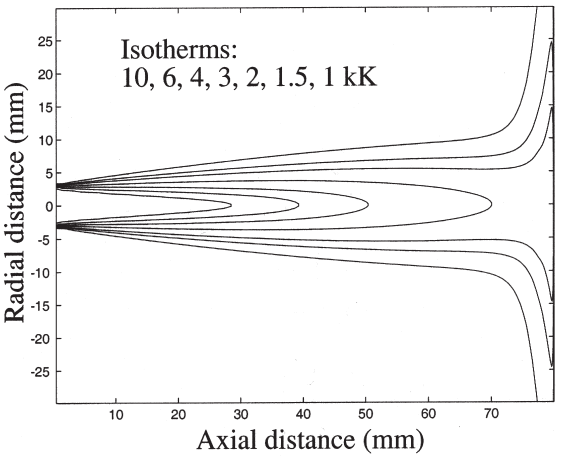


Fig. 7. View of the temperature field computed with the two-layer extension to the Chen–Kim ($k$–$\varepsilon$) model for a stand-off distance of 80 mm.

Fig. 4 presents radial profiles of the axial velocity component for different axial distances from the nozzle exit. The range of velocity in the nozzle exit region (of the order of 2000 m/s) is observed to be in quite good agreement with measurements realized by Planche et al. [32–34].

Fig. 5 shows the streamlines deviation due to the presence of the front plate and in Fig. 6 velocity vectors give further indications concerning the relative importance of the local velocity from one point to another.

A view of the temperature field over the whole jet is proposed on Fig. 7. One can observe that a significant part of the jet is not influenced by the presence of the front plate so that only a distance of the order of 1 cm is concerned by its presence. Nevertheless, the temperature

field is greatly affected by the presence of the plate in this region.

It was verified that a similarity region exists for enthalpy: in this region, radial profiles of enthalpy can be approximately deduced from velocity ones. Nevertheless, in view of the important specific heat variations of the plasmas, temperature profiles cannot be deduced from velocity ones and their shape are significantly affected.

Fig. 8 presents a comparison of the computed axial temperature profile obtained for the standard ($k$–$\varepsilon$) model that was used in [11] and the Chen–Kim one that is proposed in the present study for a stand-off distance of 80 mm. Results are also given for two different values of the turbulent Prandtl and Schmidt numbers in the case of the standard ($k$–$\varepsilon$) model. One can easily verify that the turbulence model plays an important role on the predicted profiles. Since the standard model overestimates the radial expansion of the jet, it also predicts a too fast axial temperature decrease. This being, the predicted length of the potential core increases with the values of the turbulent Prandtl and Schmidt numbers, this resulting from a decrease of the diffusive term. One can notice that computed axial temperature profiles are affected by the presence of the front plate on a shorter distance than velocity one.

The validity of the present model was tested on the basis of the comparison of predicted thermal exchanges with results obtained using the heuristic formula of Monerie-Moulin deduced from experimental measurements. In their study, Monerie-Moulin et al. [37] used two different coaxial calorimeters and measured the heat flux from the temperature increase of the cooling water circuit, which maintained a low temperature at the surface of the calorimeters. Since the diameter of the inner calorimeter was small (6.35 mm), it gave a good evaluation of the flux at the impinging point. Concerning the second calorimeter (diameter 76 mm), it was used in order to give the mean flux exchanged over its surface and mainly to deduce the radius of a Gaussian profile of the flux which would have given the same overall thermal exchange. A Gaussian shape of the flux was assumed as a first approximation in the absence of better propositions. Finally, they proposed the following correlation in order to estimate the centerline flux ($\mathrm{MW\,m^{-2}}$)

$$q_0 = 0.228 + 5.57\ 10^{-10}\mathrm{Fr}^{0.052}\mathrm{Ar}^{-1.64}d^{-2.55}p^{1.33}D^{-0.34}, \quad (2)$$

where Fr is the total plasma gas flow rate (argon+hydrogen) (l/min), Ar is the volume fraction of argon in the plasma (%), $d$ the distance from the nozzle exit to the substrate (m), $p$ the electric power (W) and $D$ is the nozzle diameter (m).

Thermal exchanges predictions corresponding to the above axial temperature profiles for the different turbulence models are given in Fig. 9. Results obtained using the Lam–Bremhorst low-Reynolds extension to the standard ($k$–$\varepsilon$) model coupled with the use of the Yap correction term are also presented. One can observe that for the same values of the turbulent Prandtl and Schmidt numbers, predictions obtained with the two-layer extension to the standard ($k$–$\varepsilon$) model are very similar to those obtained with the Lam–Bremhorst low-Reynolds extension if the Yap correction source term is used. Nevertheless, the comparison of the predicted thermal exchanges with the results obtained from the formula deduced from measurements (2.2 $\mathrm{MW\,m^{-2}}$ in the centerline region) indicates that a significant underestimation is always obtained with the standard ($k$–$\varepsilon$) model, this underestimation being related to less realistic

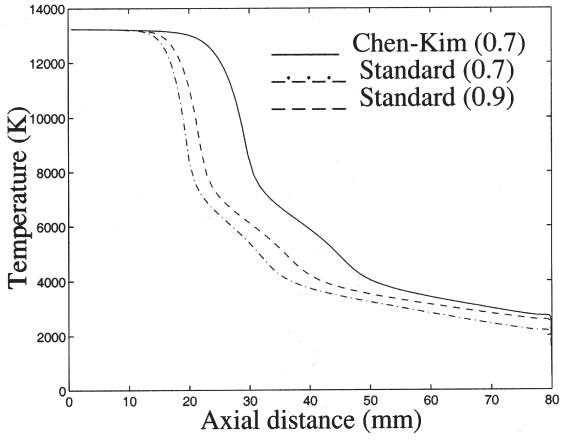


Fig. 8. Axial temperature profiles computed with the Chen–Kim ($k$–$\varepsilon$) model and the standard one for different values of the turbulent Prandtl and Schmidt numbers.

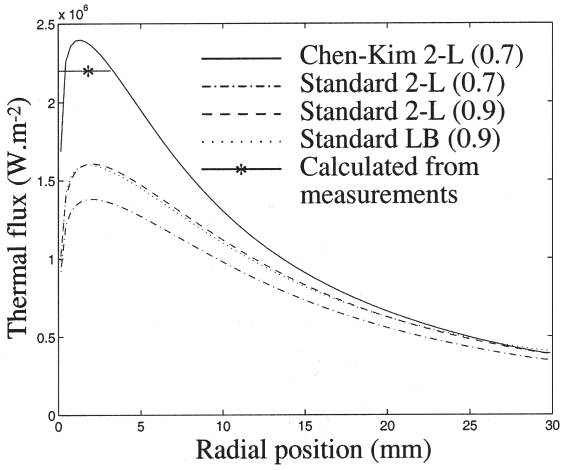


Fig. 9. Predictions of thermal exchanges using different models.

temperature and velocity fields and not to the boundary-layer description. The use of different wall functions in the impinging region (standard log law and Reichardt law of the wall) was tested in [11] for the standard ($k$–$\varepsilon$) model and was found to lead to a more important underestimation of thermal exchanges (certainly because of large property gradients in the boundary layer, the effect of which is not taken into account using wall functions). On the contrary, the use of the two-layer extension to the Chen–Kim model gives better predictions of thermal exchanges since we can assume that more realistic velocity and temperature fields are predicted.

Fig. 10 presents a comparison of the predictions of thermal exchanges with measurements (or more precisely with results obtained from the heuristic formula deduced from measurements) for the different stand-off distances proposed above and using the Chen–Kim ($k$–$\varepsilon$) model. Deduced fluxes corresponding to stand-off distances of 80, 100 and 125 mm are, respectively, of 2.2, 1.34 and 0.86 MW m$^{-2}$. Tendencies obtained with the numerical model indicate larger thermal exchanges for short stand-off distances and smaller ones for high stand-off distances, indicating a strong sensitivity regarding to the stand-off distance. Meanwhile, one can notice the difficulty to use a simple law in order to obtain thermal exchange predictions over such a large domain. For example, one could expect that the decrease of the impinging region flux with the stand-off distance depends on the initial hydrogen concentration in the jet and on the diameter of the nozzle of the torch. Moreover, one can expect that the limits of validity of the heuristic formula are reached for large stand-off distances with selected parameters since it cannot predict

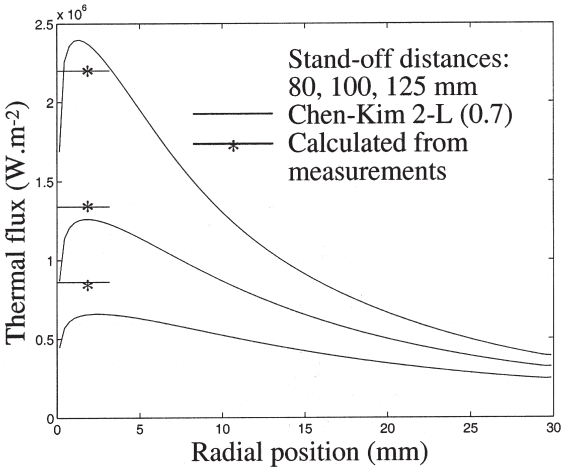


Fig. 10. Thermal exchanges computed with the two-layer extension to the Chen–Kim ($k$–$\varepsilon$) model for different stand-off distances and comparison with the centerline flux obtained from the heuritical formula of Monerie-Moulin et al. [37].

values under 0.228 MW m$^{-2}$ and this whatever the stand-off distance. Concerning the shape of the flux, as it could be expected considering the modification of the temperature field in the region close to the solid body, the Gaussian profile is not well respected. A good fitting of the numerical results could also be obtained assuming an exponential decrease (except in the centerline region) [11]. A special attention must also be paid to the fact that numerical predictions indicate maximum thermal exchanges for radial positions of the order of 2 mm from the center instead of the center point itself. That means that even if the temperature is maximum at the impinging point itself outside the boundary layer, the resulting thermal exchange coefficient is weaker at this point, leading to a smaller thermal flux. In other words, the effective thermal exchange coefficient increases with the tangential component of the velocity so that the thermal exchange is purely conductive at the impinging point since the radial velocity is zero. This result can also be related to the fact that both measurements and predictions indicate that Nusselt number profiles can present multiple maximum radially in the case of impinging jets [12,13] depending on the ratio of the nozzle diameter to the stand-off distance. For the calculations, a temperature of 300 K was assumed at the surface; nevertheless, it was verified that predicted thermal exchanges for a surface temperature of 500 K are not significantly different (the decrease in the difference of temperature between the plasma and the surface being certainly compensated by the increase of the thermal conductivity of the plasma with the temperature). The present results could thus represent the case of a structure which would be exposed during a sufficiently short time or which would be cooled so that its temperature would remain sufficiently low. Finally, pressure fields were not presented here but a quite significant increase of the pressure is also predicted in the impinging region. Computations with the Chen–Kim model indicate a relative pressure in the impinging point region of the order of 8, 5 and 3 kPa for the stand-off distances of 80, 100 and 125 mm, respectively, corresponding to an increase of 8–3% versus the absolute pressure around the system.

## 4. Conclusions

Thermodynamic properties and transport coefficients of the plasma gas mixture and of the surrounding gas were firstly calculated on the basis of chemical and thermal equilibrium assumptions. The nature of the surrounding gas (air) was taken into account by the way of a species (or mass fraction) conservation equation. Its effect is predominant concerning the cooling of the jet in the environment [1,8] due to an important part of the energy being "pumped" by the dissociation of air

molecules. Two major improvements concerning the modeling of turbulence in the case of plasma jets were established: firstly, the use of the Chen–Kim model gives a better description of velocity and temperature fields of the jet than the standard one; secondly, the use of a two-layer extension to this model leads to a better description of the relaminarization of the flow in the boundary layer and so allows a better prediction of thermal exchanges. Thus, the present model cumulates the advantages of the use of an appropriate turbulence model for round jets and the use of a good description of the viscous sublayer on the front plate. Concerning the high level of sensitivity of heat exchanges versus the stand-off distance to the solid structure, the comparison of experimental results (obtained from the heuristic formula of Monerie-Moulin et al. [37] for example) with the predictions obtained with this model can be considered to be very satisfactory and reinforce the validity of the model. It was also verified that the present model gives accurate results concerning the flux transferred to the front plate near the impinging point and also gives a good idea of the overall thermal power transmitted to a large plate [21].

## Acknowledgements

Thanks are due to Dr. Anthony B. Murphy, *SCIRO*, *Telecommunications and Industrial Physics*, *Lindfield*, *Australia* for his helpful advice concerning the calculation of transport coefficients of thermal plasmas.

## References

[1] A.B. Murphy, P. Kovitya, Mathematical model and laser-scattering temperature measurements of direct-current plasma torch discharging into air, J. Appl. Phys. 73 (10) (1993) 4759–4769.

[2] D.A. Scott, P. Kovitya, G.N. Haddad, Temperatures in the plume of a DC plasma torch, J. Appl. Phys. 66 (11) (1989) 5232–5239.

[3] A.H. Diliwari, J. Szekely, Some perspectives on the modeling of plasma jets, Plasma Chem. Plasma Proces. 7 (3) (1987) 317–337.

[4] A.H. Diliwari, J. Szekely, Fluid flow and heat transfer in plasma reactors I. Calculation of velocities temperature profiles and mixing, Int. J. Heat Mass Transfer 30 (11) (1987) 2357–3272.

[5] A.H. Diliwari, J. Szekely, R. Westoff, A comparison of experimental measurements and theoretical predictions regarding the behavior of a turbulent argon plasma jet discharging into air, Plasma Chem. Plasma Proces. 10 (4) (1990) 501–513.

[6] J.R. Fincke, C.H. Chang, W.D. Swank, D.C. Haggard, Entrainment and demixing in subsonic thermal plasma jets: comparison of measurements and predictions, Int. J. Heat Mass Transfer 37 (11) (1994) 1673–1682.

[7] C.H. Chang, J.D. Ramshaw, Modeling of nonequilibrium effects in a high-velocity nitrogen–hydrogen plasma jet, Plasma Chem. Plasma Proces. 16 (1) (1996) 5S–17S.

[8] R. Bolot, C. Coddet, M. Imbert, Mathematical modeling of a free plasma jet discharging into air and comparison with probe measurements, in: C.C. Berndt (Ed.), Thermal Spray: A United Forum for Scientific and Technological Advances, Pub. ASM International, Materials Park, OH, USA, 1997, pp. 549–555.

[9] R. Bolot, C. Coddet, M. Imbert, The use of the phoenics code for plasma jet modeling, The Phoenics J. Comput. Fluid Dynamic 10 (3) (1997) 87–104.

[10] Y.C. Lee, E. Pfender, Particle dynamics and particle heat and mass transfer in thermal plasmas. III. Thermal plasma jet reactors and multiparticle injection, Plasma Chem. Plasma Proces. 7 (1) (1987) 1–27.

[11] R. Bolot, V. Monin, M. Imbert, C. Coddet, Mathematical modeling of a plasma jet impinging on a flat structure, in: C. Coddet (Ed.), Thermal Spray: Meeting the Challenges of the 21th Century, vol. 1, Pub. ASM International, Materials Park, OH, USA, 1998, pp. 439–444.

[12] H.S. Rew, Turbulence model assessment in complex turbulent flows using phoenics, The Phoenics J. Comput. Fluid Dynamics 10 (3) (1997) 39–48.

[13] B.H. Chang, A.F. Mills, Computation of heat transfer from impinging turbulent jets, in: Proceedings of the Sixth International Conference on Transport Phenomena in Thermal Engineering, Seoul, vol. 2, Begell House, 1993, pp. 1308–1313.

[14] R.S. Amano, H. Brandt, Numerical study of turbulent axisymmetric jets impinging on a flat plate and flowing into an axisymmetric cavity, J. Fluids Eng. 106 (1984) 410–416.

[15] V.C. Patel, W. Rodi, G. Scheuerer, Turbulence models for near-wall and low Reynolds number flows: a review, AIAA J. 23 (9) (1984) 1308–1319.

[16] C. Yap, Turbulent heat and momentum transfer in recirculating and impinging flows, Ph.D. Thesis, Faculty of Technology of Manchester, 1987.

[17] W. Rodi, Experience with two-layer models combining the $k$–$\varepsilon$ model with a one-equation model near the wall, in: AIAA-91-0216, 29th Aerospaces Sciences Meeting, January 7–10, Reno, Nevada, 1991.

[18] Y.S. Chen, S.W. Kim, Computation of turbulent flows using an extented $k$–$\varepsilon$ turbulence closure model, NASA CR-179204, 1987.

[19] D. Lee, C.L. Yeh, Computation of reacting flame stabilizer flows using a zonal grid method, Numer. Heat Transfer 24 (1993) 173–285.

[20] W.R. Smith, R.W. Missen, Chemical Reaction Equilibrium Analysis: Theory and Algorithms, Wiley, New York, 1982, p. 123 (Chapter 6).

[21] R. Bolot, Modélisation des écoulements de plasmas d'arc soufflé: Application à la projection de matériaux pulvérulents, Thesis (in French), University of Franche-Comté, France, 1999.

[22] L.V. Gurvich, I.V. Veyts, C.B. Alcock, Thermodynamic Properties of Individual Substances, fourth ed., Hemisphere Washington, DC, 1989.

[23] A.B. Murphy, C.J. Arundell, Transport coefficients of argon oxygen argon–nitrogen and argon–oxygen plasmas, Plasma Chem. Plasma Proces. 14 (4) (1994) 451–489.

[24] A.B. Murphy, Transport coefficients of air, argon–air, nitrogen–air, and oxygen–air plasmas, Plasma Chem. Plasma Proces. 15 (2) (1995) 279–305.
[25] B. Pateyron, M.F. Elchinger, G. Delluc, P. Fauchais, Thermodynamic and transport properties of Ar–H2 and Ar–He plasma gases used for spraying at atmospheric pressure. I: Properties of the mixtures, Plasma Chem. Plasma Proces. 12 (4) (1992) 421–447.
[26] R. Schiestel, Modélisation et simulation des écoulements turbulents, Hermès, Paris, 1993, pp. 218, 241 (Chapters 10, 12).
[27] A. Denoirjean, O. Lagnoux, P. Fauchais, V. Sember, Oxidation control in atmospheric plasma spraying: comparison between Ar/H2/He and Ar/H2 mixtures, in: C. Coddet (Ed.), Thermal Spray Meeting the Challenges of the 21th Century, vol. 1, Pub. ASM International, Materials Park, OH, USA, 1998, pp. 809–814.
[28] M. Leylavergne, A. Vardelle, B. Dussoubs, N. Goubot, Comparison of plasma-sprayed coatings produced in argon or nitrogen atmosphere, in: C.C. Berndt (Ed.), Thermal Spray: A United Forum for Scientific and Technological Advances, Pub. ASM International, Materials Park, OH, USA, 1997, pp. 459–465.
[29] B. Dussoubs, P. Fauchais, A. Vardelle, M. Vardelle, Computational analysis of a three dimentional plasma spray jet, in: C.C. Berndt (Ed.), Thermal Spray: A United Forum for Scientific and Technological Advances, Pub. ASM International, Materials Park, OH, USA, 1997, pp. 557–565.
[30] B. Dussoub, A. Vardelle, P. Fauchais, Modeling of a Plasma Spray System, in: P. Fauchais (Ed.), Proceedings of the Fourth International Thermal Plasma Processes Conference, Pub. Begell House, Athens, 1996, p. 861.
[31] P. Nylén, J. Wigren, M.O. Hansson, A.C. Leger, An experimental and analytical study of the air plasma spraying of tribaloy 800, in: E. Lugscheider, P.A. Kammer (Eds.), Proceedings of the United Thermal Spray Conference, Düsseldorf, 1999, pp. 134–140.
[32] M.P. Planche, Contribution à l'étude des fluctuations dans une torche à plasma, Thesis (in French), University of Limoges, France, 1995.
[33] J.F. Coudert, M.P. Planche, P. Fauchais, Velocity measurement of DC plasma jets based on arc root fluctuations, Plasma Chem. Plasma Proces. 15 (1) (1995) 47–70.
[34] M.P. Planche, J.F. Coudert, P. Fauchais, Velocity measurements for arc jets produced by a DC plasma spray torch, Plasma Chem. Plasma Proces. 18 (2) (1998) 263–283.
[35] C.K.G. Lam, K. Bremhorst, A modified form of the $k$–$\varepsilon$ model for predicting wall turbulence, J. Fluids Eng. 103 (1981) 456–460.
[36] S.V. Patankar, in: W.J. Minkowyck, E.M. Sparrow (Eds.), Numerical Heat Transfer and Fluid Flow, Hemisphere, Washington, DC, 1980, p. 126 (Chapter 6).
[37] F. Monerie-Moulin, F. Gitzhofer, P. Fauchais, M. Boulos, A. Vardelle, Flux transmitted to a cold substrate by a DC Ar–H2 spraying plasma jet, J. High Temperature Chemical Processes 1 (Suppl. 3) (1992) 249–257.